Monitoring of Wettability Behaviour During Capillary Pressure Measurements at Reservoir Conditions: An Alternative Experimental Approach

Meysam Nourani*, *Mohammad* Ghasemi, *Stefano* Pruno, *Geir* Inge Høivik *and Hans-Erik* Rodvelt

Stratum Reservoir AS, Stavanger, Norway

Abstract. The development of an alternative method for monitoring wettability behaviour during capillary pressure experiments under reservoir conditions was investigated. This study aimed to address the challenges of understanding wettability dynamics, which significantly influence saturation, fluid distribution, and multiphase flow in porous media. By integrating data from various experimental techniques, the proposed method enables the determination of contact angles at different capillary pressures and saturations. Mercury injection capillary pressure (MICP) drainage cycle data, obtained under ambient conditions, was converted to representative reservoir conditions using porosity measurements at net reservoir stress and by adjusting the data to relevant fluid pairs, such as crude oil/brine systems. Additionally, interfacial tension (IFT) measurements via the pendant drop method were performed under reservoir pressure and temperature. The wettability term in the Young-Laplace capillary pressure equation was then adjusted for each capillary pressure equilibrium step to ensure that water saturation from oil-water primary drainage capillary pressure measurements matched the corresponding water saturation derived from the converted mercury-air capillary pressure data, refined using IFT and modified MICP values. For validation, contact angle measurements were conducted between reservoir crude oil, simulated formation water, and a silica surface under reservoir pressure and temperature conditions. This validation step ensures the accuracy of the estimated contact angles obtained from the integrated experimental approach. The proposed method enhances the interpretation of capillary behaviour in porous media by providing valuable insights into wettability changes as a function of sample preparation, capillary pressure versus saturation, and time during laboratory experiments, within the boundary conditions of the Young-Laplace equation.

Introduction

Capillary pressure accuracy is crucial to reservoir characterization and simulation [1,2]. Capillary pressure, defined as the difference in pressure across the interface between two immiscible fluids, directly affects fluid distribution and flow patterns within porous media. Oil/brine capillary pressure can be measured directly with techniques like the porous plate method (PcRI) and centrifugation [2]. Depending on the wettability state of a rock, capillary pressure curves, which plot pressure against water saturation, reveal significant differences [3,4]. The capillary pressure in water-wet systems is generally higher at any given saturation level than that in oil-wet systems. This can be explained by the fact that water preferentially occupies the smaller pores in water-wet systems, thereby requiring higher capillary pressure in order to displace the water with the non-wetting phase. By contrast, in oil-wet systems, oil occupies smaller pores, resulting in lower capillary pressures at a given saturation level [5,6]. Furthermore, wettability can influence hysteresis, a phenomenon characterized by the dependence of capillary pressure on the saturation path. Therefore, capillary pressure will change depending on whether saturation is achieved by drainage (displacing wetting phase with non-wetting phase) or by imbibition (displacing non-wetting phase with wetting phase) [7,8].

It is possible to visualize fluid distribution and in-situ wettability alterations at the pore scale directly using µCT scanning during fluid injection. This method enables continuous monitoring of wettability during ongoing measurements, offering valuable insights into dynamic wettability changes. The disadvantage of this method is that it is relatively expensive and time-consuming, and the interpretation of the images can be challenging [9–11]. The combination of µCT with other techniques, such as NMR, can improve the accuracy of wettability assessment by providing complementary information about the fluid properties and pore structure of the fluid [10–13]. In addition, advanced numerical modelling techniques, such as digital rock physics, incorporate information from a variety of sources to produce a comprehensive model for fluid distribution and wettability [14,15].

The wettability distributions of porous materials are inherently complex, characterized by spatial variability and influenced by dynamic forces, chemical heterogeneity, and surface roughness. While common in situ measurement techniques provide localized wettability data, they face limitations in accurately capturing the complexities of multiphase fluid interactions within voxelized three-dimensional domains. Recent advances have addressed these challenges by developing extended topological approaches to the measurement of contact angle (CA) in situ, particularly in mixed wettability

* Corresponding author: Meysam.nourani@stratumreservoir.com

domains. In addition to offering streamlined implementations and improved robustness, these methods effectively address the challenges associated with the ill-posed meshing stage while enhancing spatial resolution and complementing traditional geometric measurement techniques as well [16]. While recent progress in wettability monitoring techniques has been promising, applying these methods for extended measurements in PcRI rigs over several months to a year presents significant practical challenges.

According to the Young-Laplace equation, capillary pressure is proportional to interfacial tension (IFT) and the cosine of the CA. It is a common practice to apply the Young-Laplace equation to convert laboratory data obtained from an air–mercury system to an oil–water system at laboratory conditions. This conversion assumes that capillary pressure in rock formations can be represented using a bundle of capillary tubes [17].

Mercury injection capillary pressure (MICP) measurements, typically performed at ambient conditions, are ideally conducted on the end trim of the same core plug used for PcRI experiments. This practice facilitates direct comparison between MICP and PcRI curves, supporting in both quality control and interpretation. To ensure that PcRI data reflect representative reservoir conditions, MICP measurements should preferably be supported by IFT and CA data. However, in practice, such measurements are occasionally available, and fixed approximations for IFT and CA are commonly employed.

To address these limitations, this study presents an enhanced computational workflow grounded in the Young–Laplace equation. The proposed method incorporates experimentally measured IFT, applies corrections to MICP data, and employs a physics-informed tuning strategy to dynamically adjust the CA at each capillary pressure step. This eliminates the need for fixed or assumed values, thereby improving the reliability of the interpretation. By integrating multiple experimental datasets, the workflow enables indirect estimation of wettability during PcRI measurements, providing deeper insights into wettability alteration processes under realistic reservoir conditions.

Sample Preparations

The 1.5-inch horizontal core plugs were drilled and subjected to X-ray CT scanning to assess plug quality and ensure core sample integrity. Following this screening, only the most homogeneous and representative plugs were chosen for PcRI measurements. These selected plugs were trimmed at both ends, with one end considered for MICP analysis and the other retained as spare material. The end-trim samples were cleaned using a submerged Soxhlet extraction process, where they remained immersed in a methanol-toluene solvent to prevent evaporation and clay dehydration. After cleaning, the samples were dried at 90°C in preparation for MICP measurements. For PcRI analysis, the plugs were cleaned using a miscible solvent flooding process, involving a toluene/methanol mixture, toluene, chloroform, and methanol. This cleaning was conducted at 20 bar Net Confining Pressure (NCP) and 60°C. Subsequently, the plugs were dried in an oven at 60°C to complete the preparation process. The clean and dry core plugs were fully saturated with synthetic formation water (SFW) using vacuum and pressure techniques within single core holders to ensure complete brine saturation.

Resistivity measurements were conducted under fully saturated conditions until ionic equilibrium was attained. To introduce Stock Tank Oil (STO), primary drainage by incremental capillary pressure was performed using the porous plate method in single core holders under isostatic NCP and temperature conditions. The oil phase served as the non-wetting phase, with pressure maintained at each incremental step until equilibrium was achieved. This process allowed for the determination of oil-water capillary pressure at multiple representative capillary pressure steps under controlled NCP and temperature conditions [18].

Development of the Method

According to the Young–Laplace equation applied to a cylindrical capillary; capillary pressure is inversely related to the pore throat radius (R) [19]. The application of the Young–Laplace equation to air–mercury and oil–water systems yield Equations (1) and (2), respectively.

$$P_c = \frac{2\sigma \cos\theta}{R} \tag{1}$$

$$P_{c_{o/w}} = \frac{2\gamma_{ow} \cos\theta_{ow}}{R} \tag{2}$$

where P_c represent mercury/air capillary pressure. Here σ and θ denote the surface tension (ST) and the CA between air and mercury, respectively. Similarly, $P_{c_{o/w}}$, γ_{ow} and θ_{ow} represent the capillary pressure, the IFT and the CA between oil and water, respectively. Pore throat radius is a common variable in both equations. Therefore, by combining Equations (1) and (2), the capillary pressure between oil and water can be calculated as follows:

$$P_{c_{o/w}} = P_c \frac{\gamma_{ow} \cos\theta_{ow}}{\sigma \cos\theta} \tag{3}$$

As a best practice, mercury/air capillary pressure should be determined at the representative overburden pressure of the reservoir. However, if such data are not available, the following equations can be used to convert ambient mercury/air capillary pressure data to overburden conditions [17]:

$$P_c{}^* = P_c \left[\frac{\varphi_{res}}{\varphi_{lab}}\right]^{-0.5} \tag{4}$$

$$S_{nw}{}^* = S_{nw} \left[\frac{\varphi_{res}}{\varphi_{lab}}\right] \tag{5}$$

where $P_c{}^*$ is overburden corrected mercury/air capillary pressure, S_{nw} is ambient non-wetting phase

saturation, $S_{nw}{}^{*}$ is overburden corrected non-wetting phase (mercury) saturation, φ_{lab} is porosity measured under ambient conditions and φ_{res} is overburden corrected porosity.

Rewriting Equation (3) under the overburden condition leads to Equation (6):

$$P_{c_{o/w}}{}^{*} = P_c{}^{*} \frac{\gamma_{ow}{}^{*} cos\theta_{ow}{}^{*}}{\sigma^{*} cos\theta^{*}} \quad (6)$$

Similar to the definition of $P_c{}^{*}$, the superscript star (*) on each variable denotes its value corrected for overburden pressure effects. Combining Equations (4) and (6), the overburden corrected capillary pressure between oil and water can be calculated as follows:

$$P_{c_{o/w}}{}^{*} = P_c \left[\frac{\varphi_{res}}{\varphi_{lab}}\right]^{-0.5} \frac{\gamma_{ow}{}^{*} cos\theta_{ow}{}^{*}}{\sigma^{*} cos\theta^{*}} \quad (7)$$

The equivalent amount of water wet phase saturation at ambient and overburden pressures can be calculated using equations (8) and (9).

$$S_w = 1 - S_{nw} \quad (8)$$

$$S_w{}^{*} = 1 - S_{nw}{}^{*} \quad (9)$$

By combining Equations (5), (8) and (9), the overburden corrected water wet phase saturation is calculated as follows:

$$S_w{}^{*} = 1 - \left[\frac{(1-S_w)\varphi_{res}}{\varphi_{lab}}\right] \quad (10)$$

Under reservoir conditions, clay-bound water (CBW) occupies a portion of the pore space as water associated with clay minerals. This bound water is typically removed during the cleaning and drying process prior to MICP measurements [20]. However, the CBW correction has not been integrated into our correction workflow.

To accurately convert mercury/air capillary pressure ambient data to oil/water capillary pressure under overburden conditions using Equations (7) and (10), it is essential to have porosity measurements at both ambient and overburden conditions. Additionally, IFT must be measured at reservoir conditions. The ST and CA between air and mercury under ambient conditions are 485 mN/m [17] and 130 degrees [21], respectively. Variations in mercury-air ST and CA with pressure are deemed negligible at typical reservoir overburden pressures. Consequently, this study assumes that the ST and CA between air and mercury remain constant at 485 mN/m and 130 degrees, irrespective of overburden pressure. Consequently, the only unknown variable in equation (7) remains the cosine of the CA. By assuming the CA for each capillary pressure equilibrium step and iterating CA to find the optimal match, it is ensured that the water saturation from oil-water primary drainage capillary pressure measurements aligns with the corresponding water saturation derived from the converted mercury-air capillary pressure data. The flow chart in Figure 1 illustrates the steps required to determine the best match for CAs. In the PcRI measurement, i represents the number of pressure steps. Typically, the PcRI experiment consists of six pressure steps, so i ranges from 1 to 6. The variable j denotes the iteration of the CA for each pressure step. Initially, CA can be assumed to be zero. Using equations (7) and (10), mercury capillary pressures and saturations at ambient pressure are converted to oil-water capillary pressures under reservoir overburden pressure. The corresponding water saturation from these converted data is then compared to the water saturation from PcRI data at the specific capillary pressure step. If the absolute difference between the two water saturations is smaller than a predefined small value (ε), the selected CA is deemed the matched CA. If not, the CA is incremented by one degree, and the process iterates between zero and 89° until a match is achieved. Incrementing the CA by one degree is optional but recommended due to its sufficient accuracy. However, finer or coarser iteration steps can be used if necessary.

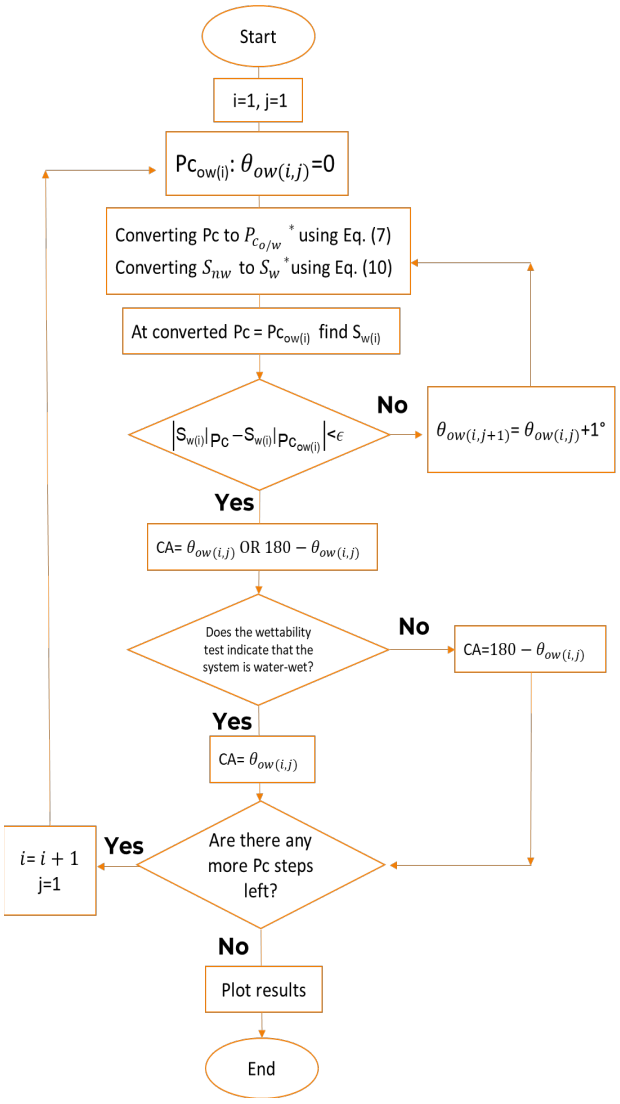

Figure 1. An overview of the steps involved in matching the CA. In the PcRI test, i represents the number of pressure steps while j represents the number of iterations required to determine the best CA fit. A single iteration step should result in an increase of one degree in CA between zero and 89 degrees.

Once a match is obtained, the availability of a wettability test result becomes important. In Equation (1), a CA of 130° results in negative capillary pressure. This is because capillary pressure is defined as the pressure of the non-wet phase minus the wet phase, indicating that the wet phase (air) pressure is greater than the non-wet (mercury) phase. However, the absolute value of the cosine of the CA is used because MICP experiments measure the external pressure required to push mercury into the sample, resulting in reported capillary pressures that are positive in magnitude, as both air and mercury are non-wetting phase by nature. In Equation (7), the absolute value of $cos\theta_{ow}{}^{*}$, is also considered. Since the absolute value of $cos\theta_{ow}{}^{*}$ is equal to the absolute value of $cos\,(180°\text{-}\theta_{ow})^{*}$, this equation mathematically yields two results: θ_{ow} and $(180°\text{-}\theta_{ow})$. In practice, only one result is correct and acceptable based on the wettability of the rock-fluid system. Equation (7) alone is unable to identify the correct result from the two options. Independent wettability test results are necessary to determine the correct result. If the wettability test indicates that the system is water wet, the accepted result is θ_{ow}. If the wettability test indicates that the system is oil wet, the accepted result is $(180°\text{-}\theta_{ow})$. When the correctly matched CA is selected based on the wettability test result, the entire calculation process is repeated for the next pressure step, $i+1$, and continues until the best logical CA match is found for all capillary pressure steps.

Results and Discussion

MICP measurements are ideally conducted on the end trim of the same core plug used for PcRI experiments. The converted MICP curve can then be plotted alongside the PcRI data to support interpretation and ensure consistency. To obtain representative PcRI measurements under reservoir conditions, it is essential to complement MICP data with accurate IFT and CA measurements. However, since these measurements are not always available, standard approximations, typically 32 mN/m for IFT and 30° for CA, are often used. For the first example, Figure 2 displays the PcRI curve for the oil-water system and the converted MICP data without overburden pressure correction. Standard literature values of 32 mN/m for IFT and 30° for CA were utilized to convert the MICP ambient data. As shown in Figure 2, the MICP converted data deviates from the PcRI data points due to the use of irrelevant IFT and CA values. The IFT value, measured using the pendant drop method under reservoir conditions, was determined to be 8.8 mN/m. This value was combined with a contact angle of 30° to convert MICP ambient data, as depicted in Figure 3. Despite correcting for overburden pressure and using the measured IFT in MICP data conversion, the MICP and PcRI curves exhibit significant deviations. This larger deviation highlights the need to use accurate contact CAs and measured IFT values instead of default values.

The Amott–Harvey index (I_{AH}) determined on the closest samples to this sample is around zero. The following linear relationship can be used to convert the Amott index to CA [22]:

$$CA° = -44.79\, I_{AH} + 89.54 \qquad (11)$$

CA ranges for water-wet, oil-wet, and neutral wettability rocks are listed in table 1 [23].

Table 1. CA ranges for water-wet, oil-wet, and neutral wettability rocks [23].

CA	Oil wet	Water wet	Neutrally wet
Max. value	180°	60°–75°	105°-120°
Min. value	105°-120°	0°	60°-75°

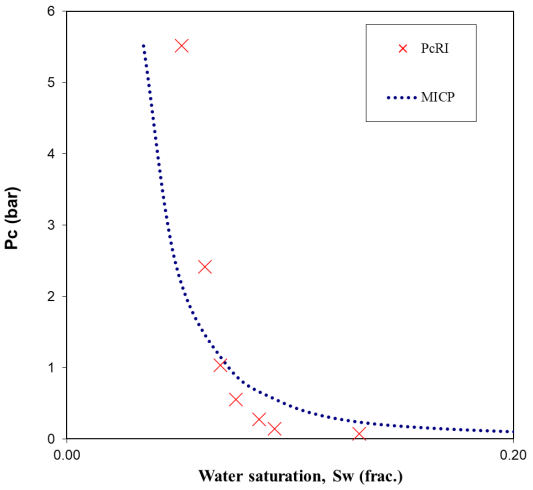

Figure 2. Example 1, comparison of PcRI and converted MICP data. The MICP data is presented without applying overburden pressure correction, using standard values of 32 mN/m for IFT and 30° for CA to convert MICP ambient data.

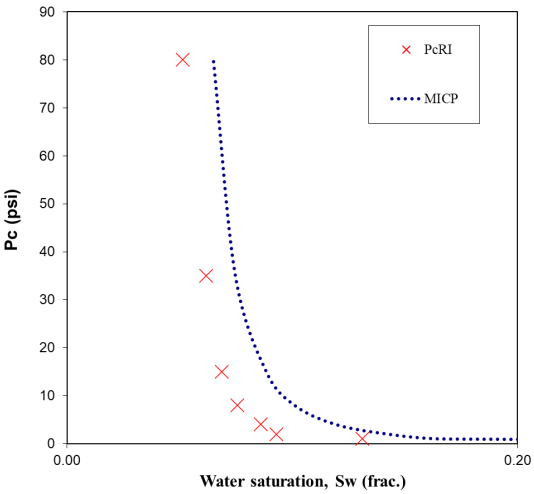

Figure 3. Example 1, comparison of PcRI and converted MICP data. The MICP data is presented with overburden pressure correction applied, using a measured value of 8.8 mN/m for IFT and the standard 30° for CA to convert MICP ambient data.

Using Equation (11), the CA for this sample is estimated to be around 90°, which falls within the range of neutral wettability conditions. PcRI measurements are inherently time-intensive, with a complete drainage cycle often taking several months to over a year, depending on the rock type and its properties. Prolonged exposure of the sample to reservoir pressure and temperature conditions over such extended periods can lead to changes in wettability, potentially shifting it toward a more oil-wet state. Using the CA matching procedure, the calculated CAs are 71° and 109° for the first capillary pressure step. Given that the sample was cleaned by low-rate solvents flooding, it should be water-wet at the beginning of the PcRI measurement. Therefore, the CA of 71°, which falls within the water-wet region, is considered valid. For the second capillary pressure step, the matched CAs are 82° and 98°, both of which fall within the neutral wettability range. Following the same procedure and approach, the matched and accepted CAs for all 6 pressure steps are shown in Figure 4. Figure 4 demonstrates how the matching CA method effectively aligns the MICP-converted data with the PcRI curve.

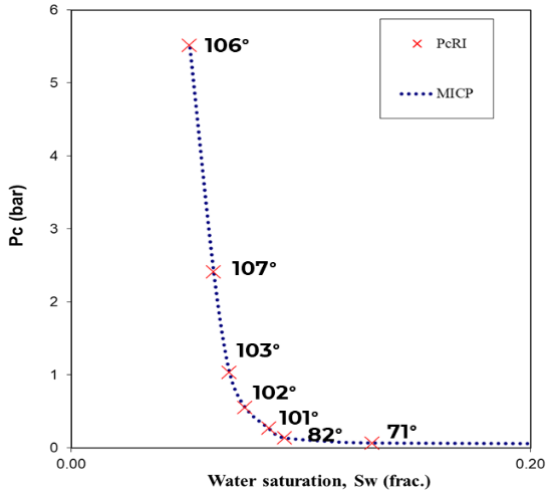

Figure 4. Example 1, comparison of PcRI and converted MICP data. The MICP data is presented with overburden pressure correction applied, using a measured value of 8.8 mN/m for IFT and the matched CAs to convert MICP ambient data.

In the second example using the same fluid system on another sample, the I_{AH} index is 0.93, which falls within the water-wet region. Equation (11) was used to calculate the equivalent contact angle of 48°. Figure 5 illustrates the converted MICP data for this example, using measured IFT and matched CAs in accordance with the water-wet state.

Figure 6 illustrates a robust correlation between water saturation values derived from MICP data, converted using matched contact angles CAs, and those obtained from PcRI measurements for four samples within the same fluid system in examples 1 and 2. This correlation is verified by a coefficient of determination (R^2) of 0.9997.

As discussed, an independent wettability test guideline is necessary to select the valid CA between two matched options. The two most commonly used wettability indices are the AH index and the U.S. Bureau of Mines (USBM) wettability index [24–26]. Both indices are related to CA but require conversion through correlations. Additionally, both methods necessitate twin samples for measurements and are time-consuming. Therefore, directly measuring CA under reservoir conditions appears to be a more efficient approach. However, the challenge with CA measurement lies in the inherent roughness and chemical heterogeneity of reservoir rock samples, necessitating a distinction between the true CA and the apparent CA.

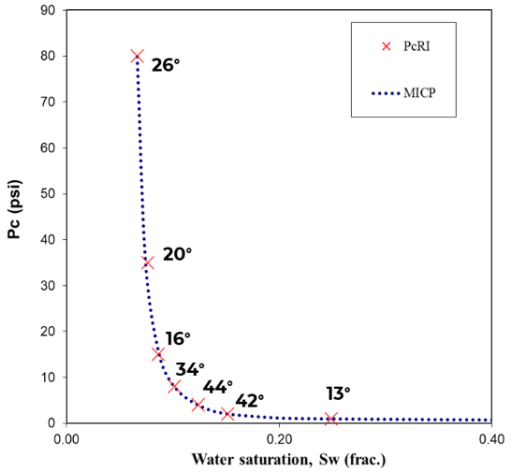

Figure 5. Example 2, comparison of PcRI and converted MICP data. The MICP data is presented with overburden pressure correction applied, using a measured value of 8.8 mN/m for IFT and the matched CAs to convert MICP ambient data.

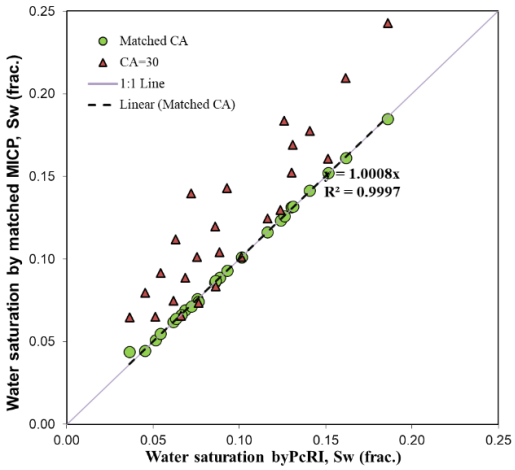

Figure 6. Water saturation by matched MICP versus water saturation by PcRI measurements for 4 samples with oil water fluid system.

A proposed solution to overcome this challenge is to conduct CA measurement on silica-coated quartz crystal microbalance (QCM) sensors to simulate the smooth and ideal surface of sandstone reservoirs. The QCM sensors are composed of a thin disk of single-crystal quartz, with metal electrodes deposited on both sides of the disk [27–29]. In this study, QCM sensors coated with silicon dioxide (QSX 303, QSense) were employed for independent CA measurements as shown in Figure 7.

The third PcRI experiment was performed on a sandstone rock sample using a fluid system distinct from

those employed in the previous examples. The measurement was conducted over a period of eight months under NCP and reservoir temperature conditions. Figure 8 presents the CA measurement between oil, brine, and a silica-coated QCM surface under these conditions. The measured CA of 158° indicates a strongly oil-wet system, with oil demonstrating a clear preference for adhesion to the silica surface.

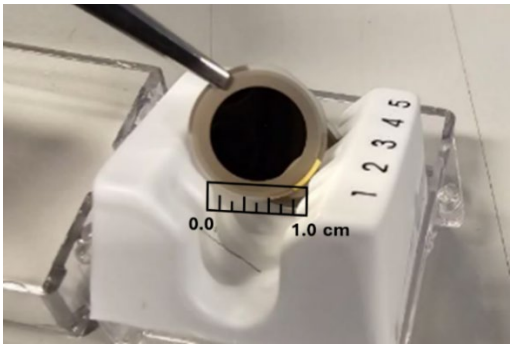

Figure 7. Image of a QCM sensor coated with silicon dioxide, used as a synthetic rock surface for independent CA measurements. The QCM sensor has a dimension of 1 cm.

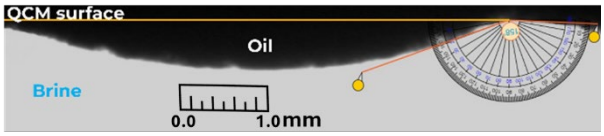

Figure 8. Illustration of the high CA, 158°, between oil, water, and a silica-coated crystal surface under reservoir pressure and temperature conditions. The oil droplet spreads on the surface, indicating preferential adhesion of oil to the solid.

The IFT value was measured using the pendant drop method under reservoir conditions to be 19.3 mN/m. For the third example, Figure 9 shows the converted MICP using the measured IFT and matched CAs in accordance with the oil-wet guideline derived from the independent CA measurement shown in Figure 8. Figure 9 shows that the MICP matched curve for the first three pressure steps aligns well with the PcRI data, while a slight deviation is observed in the last three pressure steps. This deviation most likely occurs because of changes in wettability towards oil-wet conditions also affect the IFT. One of the possible mechanisms could be that as surface-active components transfer from the fluid interfaces to the silica surfaces, the IFT increases concurrently with the shift towards a more oil-wet state. Figure 10 illustrates the linear relationship between the matched CA and oil saturations. It is assumed that, following cleaning with organic solvents and re-saturating the sample with SFW, the sample was initially water-wet and fully saturated with water. As oil was injected and oil saturation increased over time, the concentration of oil polar components in the sample rose, leading to a shift towards a more oil-wet condition. Figure 11 shows that increasing the IFT to 22.3 mN/m for the fourth pressure step results in a well-matched correlation between the saturations of converted MICP and PcRI data. Similarly, for the fifth and sixth pressure steps, IFT values of 27.3 mN/m and 28.3 mN/m, respectively, led to matched CAs.

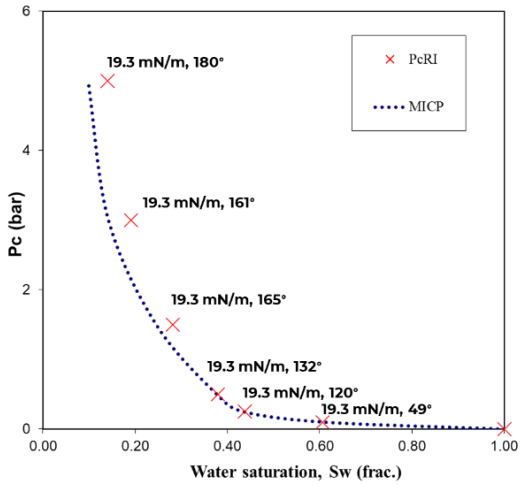

Figure 9. Example 3, comparison of PcRI and converted MICP data. The MICP data is presented with overburden pressure correction applied, using a measured value of 19.3 mN/m for IFT and the matched CAs to convert MICP ambient data.

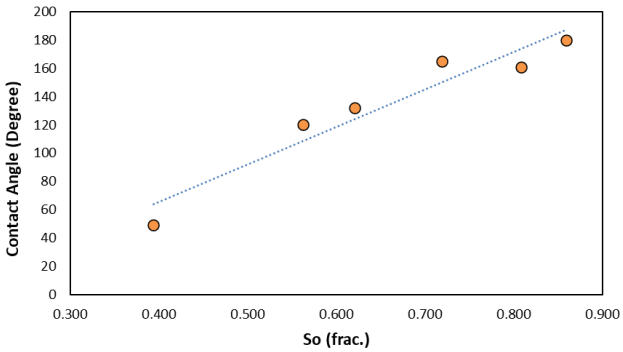

Figure 10. Example 3, matched CAs using measured IFT versus oil saturations for data of the second sample shown in Figure 9.

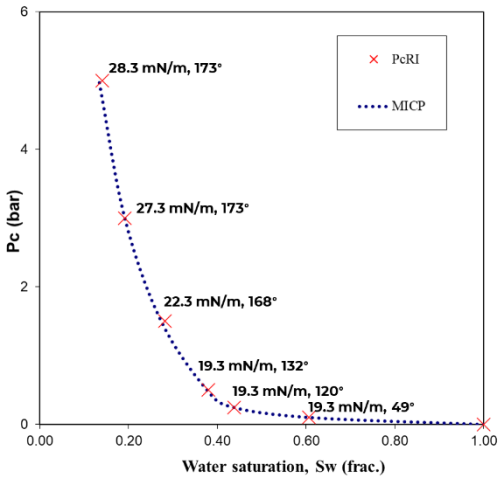

Figure 11. Example 3, comparison of PcRI and converted MICP data. The MICP data is presented with overburden pressure correction applied, using a matched IFT and the matched CAs to convert MICP ambient data, while using 19.3 mN/m as the initial guess.

Conclusions

A tailored calculation method, derived from the Young-Laplace equation, has been developed to elucidate wettability dynamics during capillary pressure measurements under reservoir conditions. This method integrates multiple experimental techniques to capture wettability alteration during oil/water capillary pressure measurements. For the developed method to be operational, the porosity of the sample must be measured under both ambient and reservoir pressure conditions. Additionally, IFT measurement at reservoir conditions is required, along with the result of a wettability test.

The availability of independent wettability test results is critical, as the model mathematically yields two CAs, both of which may be valid. To illustrate, consider an analogue clock displaying 2 o'clock. It is ambiguous whether this indicates 2 o'clock in the morning or afternoon. The correct time can be determined by consulting an external reference, such as the position of the sun. For example, darkness suggests 2 o'clock in the morning, while daylight indicates 2 o'clock in the afternoon. However, the analogue clock itself cannot independently resolve this ambiguity. In this study, CA measurement with reservoir fluids under reservoir conditions conducted on the surface of the QCM sensor to determine the correct matched CA. The validity of this approach was confirmed through comparisons of water saturation values derived from MICP data, adjusted using matched CAs, and those obtained from PcRI measurements. The results demonstrated a strong correlation between the datasets. However, deviations ranging from 13% to 31%, with a Mean Squared Error (MSE) of 0.001875, were observed at higher capillary pressures, particularly during the transition from a water wet to an oil-wet system. These deviations are most likely to be attributed to the simultaneous change in IFT as surface-active components migrate from fluid interfaces to surfaces, corresponding with the shift towards a more oil-wet state.

Acknowledgment

The authors extend their gratitude to Vår Energi ASA for granting permission to publish some data in this paper and would like to especially thank Subhadeep Sarkar for his valuable support and assistance throughout the course of this work. Fruitful discussions and constructive feedback provided by Min Cheng (Stratum Reservoir, USA) were highly appreciated and contributed to the improvement of this work.

References

1. Jiao L, Zhou J, Cai J. Applications of mercury intrusion capillary pressure for pore structures: A review. Capillarity 3, 62–74 (2020).
2. Green D.P., Dick J.R., McAloon M., Cano-Barrita P.F. de J., Burger J., Balcom B., et al. Oil/water imbibition and drainage capillary pressure determined by MRI on a wide sampling of rocks. SCA Conf., Abu Dhabi, UAE, vol. 29, Citeseer (2008).
3. Falode O., Manuel E. Wettability effects on capillary pressure, relative permeability, and irreducible saturation using porous plate. J. Pet. Eng. 2014, 465418.
4. Pini R., Benson S.M. Simultaneous determination of capillary pressure and relative permeability curves from core-flooding experiments with various fluid pairs. Water Resour. Res. 49, 3516–30 (2013).
5. Graue A., Bognø T., Moe R.W., Baldwin B.A., Spinler E.A., Maloney D., et al. Impacts of wettability on capillary pressure and relative permeability. SCA9907, Int. Symp. Core Analysts, Golden, CO, USA (1999).
6. Garing C., Benson S.M. CO_2 wettability of sandstones: Addressing conflicting capillary behaviors. Geophys. Res. Lett. 46, 776–82 (2019).
7. Elashahab B.M., Jing X.D., Archer J.S. Resistivity index and capillary pressure hysteresis for rock samples of different wettability characteristics. SPE Middle East Oil Gas Show Conf., SPE-29888 (1995).
8. Dernaika M.R., Kalam M.Z., Basioni M.A., Skjæveland S.M. Hysteresis of capillary pressure, resistivity index and relative permeability in different carbonate rock types. Petrophysics 53, 316–32 (2012).
9. AlRatrout A., Blunt M.J., Bijeljic B. Spatial correlation of contact angle and curvature in pore-space images. Water Resour. Res. 54, 6133–52 (2018).
10. Alhammadi A.M., Gao Y., Akai T., Blunt M.J., Bijeljic B. Pore-scale X-ray imaging with measurement of relative permeability, capillary pressure and oil recovery in a mixed-wet micro-porous carbonate reservoir rock. Fuel 268, 117018 (2020).
11. Boon M., Hajibeygi H. Experimental characterization of H_2/water multiphase flow in heterogeneous sandstone rock at the core scale relevant for underground hydrogen storage (UHS). Sci. Rep. 12, 14604 (2022).
12. Mohnke O. Jointly deriving NMR surface relaxivity and pore size distributions by NMR relaxation experiments on partially desaturated rocks. Water Resour. Res. 50, 5309–21 (2014).
13. Li Y., Li H., Cai J., Ma Q., Zhang J. The dynamic effect in capillary pressure during the displacement process in ultra-low permeability sandstone reservoirs. Capillarity 1, 11–8 (2018).
14. Shikhov I., Arns C.H. Evaluation of capillary pressure methods via digital rock simulations. Transp. Porous Media 107, 623–40 (2015).
15. Kalam M.Z. Digital rock physics for fast and accurate special core analysis in carbonates. New Technol. Oil Gas Ind. 2012, 201–26.
16. Da Wang Y., Kearney L.M., Blunt M.J., Sun C., Tang K., Mostaghimi P., et al. In situ characterization of heterogeneous surface wetting in porous materials. Adv. Colloid Interface Sci. 326, 103122 (2024).
17. McPhee C., Reed J., Zubizarreta I. Core analysis: a best practice guide. Elsevier (2015).
18. Pruno S., Rodvelt H.E., Skjæveland O. Measurement of spontaneous imbibition capillary pressure, saturation and resistivity index by counter current

technique at net reservoir stress and elevated temperature. E3S Web Conf. 89, 02002 (2019).
19. AAWG A.P. Physical chemistry of surfaces. Wiley784 (1997).
20. Hill H.J., Klein G.E., Shirley O.J., Thomas E.C., Waxman W.H. Bound water in shaly sands—its relation to Q and other formation properties. Log Anal. 20 (1979).
21. Brabazon D., Raffer A. Chapter 3 - Advanced characterization techniques for nanostructures. In: Ahmed W., Jackson M.J., eds. Emerging Nanotechnol. Manuf. (2nd ed.), Boston: William Andrew Publ., 53–85 (2015).
22. Nourani M., Schovsbo N.H., Ghahfarokhi A.J., Nielsen C.M., Sigalas L., Meyer A.G., et al. A predictive model for the wettability of chalk. SN Appl. Sci. 2, 1–12 (2020).
23. Anderson W.G. Wettability literature survey—part 4: Effects of wettability on capillary pressure. J. Pet. Technol. 39, 1283–300 (1987).
24. Bolysbek D., Uzbekaliyev K., Assilbekov B. Rock wettability alteration induced by the injection of various fluids: A review. Appl. Sci. 14, 8663 (2024).
25. Donaldson E.C., Thomas R.D., Lorenz P.B. Wettability determination and its effect on recovery efficiency. SPE J. 9, 13–20 (1969).
26. Amott E. Observations relating to the wettability of porous rock. Trans. AIME 216, 156–62 (1959).
27. Nourani M., Tichelkamp T., Gaweł B., Øye G. Method for determining the amount of crude oil desorbed from silica and aluminosilica surfaces upon exposure to combined low-salinity water and surfactant solutions. Energy Fuels 28, 1884–9 (2014).
28. Nourani M., Tichelkamp T., Gaweł B., Øye G. Desorption of crude oil components from silica and aluminosilicate surfaces upon exposure to aqueous low salinity and surfactant solutions. Fuel 180, 1–8 (2016).
29. Farooq U., Nourani M., Ivol F., Årrestad A.B., Øye G. Adsorption of crude oil components on mineral surfaces followed by quartz crystal microbalance and contact angle measurements: The effect of oil composition, simulated weathering and dispersants. Energy Fuels 33, 2359–65 (2019).